J. Fluid Mech. (1979), *vol.* 90, *part* 4, *pp.* 609–624
Printed in Great Britain

Nonlinear thermal convection in anisotropic porous media

By ODDMUND KVERNVOLD
AND PEDER A. TYVAND
Department of Mechanics, University of Oslo,
Blindern, Oslo 3, Norway

(Received 4 October 1977 and in revised form 15 May 1978)

In this paper a theoretical investigation of convection currents in anisotropic porous media is performed. The porous layer is homogeneous and bounded by two infinite perfectly heat-conducting horizontal planes. The criterion for the onset of convection is derived. The supercritical steady two-dimensional motion, the heat transport and the stability of the motion are investigated. Some of the results may be applied in insulation techniques.

1. Introduction

Free thermal convection in porous media has received considerable interest owing to its technical and geophysical applications. So far, theoretical and experimental investigations have usually been concerned with isotropic porous media. However, in many problems the porous materials are anisotropic. This is the case for fibrous insulation materials, where convection currents may occur. Another important example is groundwater motion in sediments and other anisotropic rocks, especially in areas with geothermal activity.

In most materials anisotropy in permeability is more pronounced than anisotropy in thermal diffusivity. This has been shown theoretically by Neale (1977) for the case of a thermally insulating matrix. For a conducting matrix no general conclusion can be drawn. Actually, anisotropy in thermal diffusivity can easily be made important by introducing thin parallel copper threads into the matrix. They can increase the diffusivity of the medium in their direction of alignment considerably, without influencing either the diffusivity in other directions or the permeability significantly.

The papers on convection in anisotropic media are recent and not numerous. Castinel & Combarnous (1975) derived the stability criterion for porous media with anisotropic permeability and made experiments concerning the supercritical heat transport and temperature field. Epherre (1975) extended the stability analysis to media with anisotropy in the thermal diffusivity also, and Tyvand (1977) took into account the effect of hydrodynamic dispersion caused by a uniform basic flow. Burns, Chow & Tien (1977) incorporated anisotropic permeability in their study of convection in vertical slots. Their study is relevant to insulation between walls, while the present study is relevant to insulation between floors and ceilings in buildings.

Nonlinear convection in isotropic porous media was treated numerically by Elder (1967), Straus (1974) and Kvernvold (1975), and analytically by Palm, Weber & Kvernvold (1972).

In this paper the onset of convection is analysed for more general types of anisotropy

than in the papers by Castinel & Combarnous (1975) and Epherre (1975). Moreover, the effects of anisotropy on the supercritical motion and the heat transfer are analysed. The stability of the steady two-dimensional motion is also analysed. In the interpretation of the results we shall concentrate on some insulating properties.

2. Governing equations

We consider free thermal convection in a homogeneous porous layer saturated by a homogeneous fluid. The layer is bounded above and below by two infinite and impermeable perfectly heat-conducting horizontal planes. The planes are separated by a distance h and have constant temperatures T_0 and $T_0-\Delta T$, the lower plane being the warmer. The saturated porous medium is assumed to have coinciding principal axes of permeability and thermal diffusivity. One of these axes is directed upwards, in the z direction. The x and y axes are defined by the directions of the other two principal axes. K_1, K_2 and K_3 are the components of the permeability in the x, y and z directions, respectively. Similarly, κ_{m1}, κ_{m2} and κ_{m3} denote the components of the diffusivity for the mixture of solid and fluid.

We choose

$$h, \quad (c_p\rho)_m h^2/\lambda_{m3}, \quad \kappa_{m3}/h, \quad \Delta T, \quad \rho_0 \nu \kappa_{m3}/K_3 \tag{2.1}$$

as units for length, time, velocity, temperature and pressure, respectively. c_p is the specific heat at constant pressure, ρ the density, ρ_0 a standard density and λ_{m3} the thermal conductivity in the z direction. The governing equations in dimensionless form may then be written as (Bear 1972, p. 652)

$$\mathbf{v}+\mathscr{K}.(\nabla p - R T\mathbf{k}) = 0, \tag{2.2}$$

$$\nabla.\mathbf{v} = 0, \tag{2.3}$$

$$\partial T/\partial t + \mathbf{v}.\nabla T = \nabla.(\mathscr{D}.\nabla T). \tag{2.4}$$

Here Darcy's law and the Boussinesq approximation have been used and the density is assumed to be a linear function of the temperature T. The other fluid properties are assumed constant. t is the time and $\mathbf{v}$ $(=u\mathbf{i}+v\mathbf{j}+w\mathbf{k})$ is the velocity, where $\mathbf{i}$, $\mathbf{j}$ and $\mathbf{k}$ denote the unit vectors in the x, y and z directions, respectively. R is the Rayleigh number defined as

$$R = K_3 g\gamma \Delta T h/\kappa_{m3}\nu, \tag{2.5}$$

where g is the acceleration due to gravity and γ is the coefficient of thermal expansion. $\mathscr{K}$ and $\mathscr{D}$ are dimensionless tensors of permeability and thermal diffusivity, respectively, and will be written as

$$\mathscr{K} = \xi_1 \mathbf{i}\mathbf{i} + \xi_2 \mathbf{j}\mathbf{j} + \mathbf{k}\mathbf{k}, \tag{2.6}$$

$$\mathscr{D} = \eta_1 \mathbf{i}\mathbf{i} + \eta_2 \mathbf{j}\mathbf{j} + \mathbf{k}\mathbf{k}, \tag{2.7}$$

where

$$\xi_1 = K_1/K_3, \quad \xi_2 = K_2/K_3, \quad \eta_1 = \kappa_{m1}/\kappa_{m3}, \quad \eta_2 = \kappa_{m2}/\kappa_{m3}. \tag{2.8}$$

By eliminating the pressure from (2.2) and substituting the field variables written as

$$T = T_0/\Delta T - z + \theta(x,y,z,t), \quad \mathbf{v} = \mathbf{v}(x,y,z,t) \tag{2.9}$$

into (2.2)–(2.4), we obtain the following equations:

$$\left(\xi_1 \frac{\partial^2}{\partial x^2} + \xi_2 \frac{\partial^2}{\partial y^2} + \frac{\partial^2}{\partial z^2}\right) w = R \left(\xi_1 \frac{\partial^2}{\partial x^2} + \xi_2 \frac{\partial^2}{\partial y^2}\right) \theta, \tag{2.10}$$

$$\nabla . \mathbf{v} = 0, \tag{2.11}$$

$$-w + \mathbf{v} . \nabla \theta = \left(\eta_1 \frac{\partial^2}{\partial x^2} + \eta_2 \frac{\partial^2}{\partial y^2} + \frac{\partial^2}{\partial z^2} - \frac{\partial}{\partial t}\right) \theta. \tag{2.12}$$

The requirements of perfectly heat-conducting and impermeable boundaries yield the boundary conditions

$$\theta = w = 0 \quad \text{at} \quad z = 0, 1. \tag{2.13}$$

3. Linear theory

The onset of convection is described by the linear version of (2.10)–(2.13). We introduce

$$\left.\begin{aligned} w &\sim e^{\sigma t} \sin \pi z \exp [i(kx + ly)], \\ \theta &\sim e^{\sigma t} \sin \pi z \exp [i(kx + ly)], \end{aligned}\right\} \tag{3.1}$$

where k and l are the wavenumbers in x and y direction, respectively. σ is the growth rate of the perturbation. The linear problem is easily shown to be self-adjoint. Then σ is real and marginal stability is given by $\sigma = 0$. The Rayleigh number for the onset of convection is found to be

$$R = \frac{\xi_1 k^2 + \xi_1 l^2 + \pi^2}{\xi_1 k^2 + \xi_2 l^2} (\eta_1 k^2 + \eta_2 l^2 + \pi^2). \tag{3.2}$$

Minimizing (3.2) with respect to k and l yields the critical Rayleigh number

$$R_c = \pi^2 \left(\min \left\{\left(\frac{\eta_1}{\xi_1}\right)^{\frac{1}{2}}, \left(\frac{\eta_2}{\xi_2}\right)^{\frac{1}{2}}\right\} + 1\right)^2. \tag{3.3}$$

We then have three cases.

Case A: $$\eta_1/\xi_1 < \eta_2/\xi_2. \tag{3.4}$$

Here the critical wavenumbers are

$$k_c = \pi(\xi_1 \eta_1)^{-\frac{1}{4}}, \quad l_c = 0, \tag{3.5}$$

which give rolls aligned in the y direction.

Case B: $$\eta_1/\xi_1 > \eta_2/\xi_2. \tag{3.6}$$

Here the critical wavenumbers are

$$k_c = 0, \quad l_c = \pi(\xi_2 \eta_2)^{-\frac{1}{4}}, \tag{3.7}$$

which define rolls aligned in the x direction.

Case C: $$\eta_1/\xi_1 = \eta_2/\xi_2. \tag{3.8}$$

Here the orientation of the rolls is undetermined. The critical wavenumber vector

$$\boldsymbol{\alpha}_c = k_c \mathbf{i} + l_c \mathbf{j} \tag{3.9}$$

is constrained by the relation

$$(\xi_1 \eta_1)^{\frac{1}{2}} k_c^2 + (\xi_2 \eta_2)^{\frac{1}{2}} l_c^2 = \pi^2. \tag{3.10}$$

In the case of horizontal isotropy, i.e.

$$\xi_1 = \xi_2 = \xi, \quad \eta_1 = \eta_2 = \eta, \tag{3.11}$$

the results reduce to

$$\left.\begin{aligned} R_c &= \pi^2[(\eta/\xi)^{\frac{1}{2}} + 1]^2, \\ \alpha_c &= (k_c^2 + l_c^2)^{\frac{1}{2}} = \pi(\xi\eta)^{-\frac{1}{4}}, \end{aligned}\right\} \tag{3.12}$$

which were first obtained by Epherre (1975).

4. Mathematical simplification of the nonlinear problem

To examine the motion for supercritical Rayleigh numbers, it proves useful to apply the following transformation to the governing equations:

$$\left[\begin{pmatrix} x \\ u \end{pmatrix}, \begin{pmatrix} y \\ v \end{pmatrix}, \begin{pmatrix} z \\ w \end{pmatrix}, \theta\right] = \left[(\xi_1\eta_1)^{\frac{1}{4}}\begin{pmatrix} x^* \\ u^* \end{pmatrix}, \quad (\xi_2\eta_2)^{\frac{1}{4}}\begin{pmatrix} y^* \\ v^* \end{pmatrix}, \begin{pmatrix} z^* \\ w^* \end{pmatrix}, \theta^*\right]. \tag{4.1}$$

In the transformed system of equations the anisotropy parameters appear only as ratios ξ_1/η_1 and ξ_2/η_2. Accordingly, $\mathbf{v}^*$ and θ^* are functions of ξ_1/η_1 and ξ_2/η_2. Without loss of generality, one of the parameters in each ratio can be put equal to 1. The mathematics will be simplified if we put $\xi_1 = \xi_2 = 1$. Then, by making the inverse transformation, the equation of motion (2.2) reduces to

$$\mathbf{v} + \nabla p - RT\mathbf{k} = 0, \tag{4.2}$$

which implies $\mathbf{k} \cdot \nabla \times \mathbf{v} = 0$. Together with $\nabla \cdot \mathbf{v} = 0$, this means that the velocity is a poloidal vector given by a single scalar function ψ as

$$\mathbf{v} = \nabla \times (\nabla \times \mathbf{k}\psi) = (\psi_{xz}, \psi_{yz}, -\nabla_1^2\psi) \equiv \boldsymbol{\delta}\psi. \tag{4.3}$$

From (2.10) the temperature field is given by

$$\theta = -R^{-1}\nabla^2\psi. \tag{4.4}$$

Introducing (4.3) and (4.4) into the heat equation (2.12), we finally obtain

$$\left[\left(\eta_1\frac{\partial^2}{\partial x^2} + \eta_2\frac{\partial^2}{\partial y^2} + \frac{\partial^2}{\partial z^2} - \frac{\partial}{\partial t}\right)\nabla^2 + R\nabla_1^2\right]\psi = \boldsymbol{\delta}\psi \cdot \nabla\nabla^2\psi. \tag{4.5}$$

The boundary conditions (2.13) are expressed as

$$\psi = \psi_{zz} = 0 \quad \text{at} \quad z = 0, 1. \tag{4.6}$$

The solutions of the above equations are transformed to give $\mathbf{v}^*$ and θ^*. Then the anisotropy in permeability is incorporated by replacing η_1 and η_2 by η_1/ξ_1 and η_2/ξ_2, respectively. We notice that physical quantities such as the velocity and temperature distributions and the size of the cells depend on the four anisotropy parameters separately, not just the two ratios. However, mean quantities such as the Nusselt number

$$Nu = 1 - [\partial\bar{\theta}/\partial z]_{z=0} \tag{4.7}$$

(the overbar denoting a horizontal average), the critical Rayleigh number and the time variation depend only on the ratios ξ_1/η_1 and ξ_2/η_2.

5. Numerical solution of the steady nonlinear problem

In anisotropic media with $\xi_1/\eta_1 \neq \xi_2/\eta_2$ (cases A and B) linear theory predicts two-dimensional motion. In media with $\xi_1/\eta_1 = \xi_2/\eta_2$ (case C) linear theory does not determine any particular horizontal planform. In this case, however, a stability analysis of the nonlinear steady motion analogous to that of Schlüter, Lortz & Busse (1965) shows that only two-dimensional motion is stable for small supercritical Rayleigh numbers. We shall therefore consider only two-dimensional motion in all three cases.

Without loss of generality, we shall assume $\xi_1/\eta_1 \geqslant \xi_2/\eta_2$ from now on. This implies that the rolls are oriented along the y axis. The steady problem is then described by assuming $\partial/\partial t = \partial/\partial y = 0$ in (4.5).

For small supercritical Rayleigh numbers the problem may be solved analytically; see the appendix. For larger supercritical Rayleigh numbers numerical methods must be applied. Using Galerkin's method, the steady solution of (4.5) subject to the boundary conditions (4.6) may be written as

$$\psi = \sum_{n=-\infty}^{\infty} \sum_{m=1}^{\infty} A_{nm} \exp(in\alpha x) \sin m\pi z, \tag{5.1}$$

where each term in the series satisfies the boundary conditions (4.7). The symmetry of the problem implies the restriction

$$A_{nm} = A_{-nm}, \tag{5.2}$$

corresponding to convection cells which are not tilted.

To determine the unknown amplitudes A_{nm}, we substitute (5.1) into (4.5), multiply by $\exp(-ip\alpha x) \sin q\pi z$ and average over the whole fluid layer. We then obtain an infinite set of algebraic equations for the A_{nm}:

$$\begin{aligned}
&((\eta_1^2 n^2\alpha^2 + m^2\pi^2)(n^2\alpha^2 + m^2\pi^2) - Rn^2\alpha^2) A_{nm} \\
&- \tfrac{1}{2} \sum_{p,q} s_{m,q} A_{n-p,(m-q)s_{m,q}} A_{pq} (p^2\alpha^2 + q^2\pi^2)(pm - qn)(n-p)\alpha^2\pi \\
&- \tfrac{1}{2} \sum_{p,q} A_{n-p,m+q} A_{pq} (p^2\alpha^2 + q^2\pi^2)(pm + qn)(n-p)\alpha^2\pi = 0,
\end{aligned} \tag{5.3}$$

where

$$s_{m,q} = \begin{cases} \pm 1 & \text{for} \quad m \gtrless q, \\ 0 & \text{for} \quad m = 0. \end{cases} \tag{5.4}$$

In order to solve these equations, it is necessary to truncate the series (5.1). We choose to neglect all terms with

$$|n| + \tfrac{1}{2}(m+1) > N, \tag{5.5}$$

where N is a sufficiently large number. Because of the symmetry in (5.3), the solution will contain only amplitudes with $n+m$ even, giving $\frac{1}{2}N(N+1)$ equations to be solved. For a given N the algebraic equations are solved by a Newton–Raphson iteration procedure. Usually we need less than five iterations to obtain a satisfactorily exact solution.

The truncation parameter N is determined by assuming the solution to be sufficiently accurate if replacing N by $N+1$ produces a change in the Nusselt number Nu of less than 1 %. Table 1 shows the variation of the Nusselt number with N for some characteristic cases.

N	$R/R_c = 8, \xi_1/\eta_1 = 1,$ $\alpha/\alpha_c = 2{\cdot}5$	$R/R_c = 12{\cdot}5, \xi_1/\eta_1 = 10,$ $\alpha/\alpha_c = 4$
6	5·23	6·93
7	5·27	7·22
8	5·29	7·37
9	—	7·45

TABLE 1. The variation of the Nusselt number with the truncation parameter N.

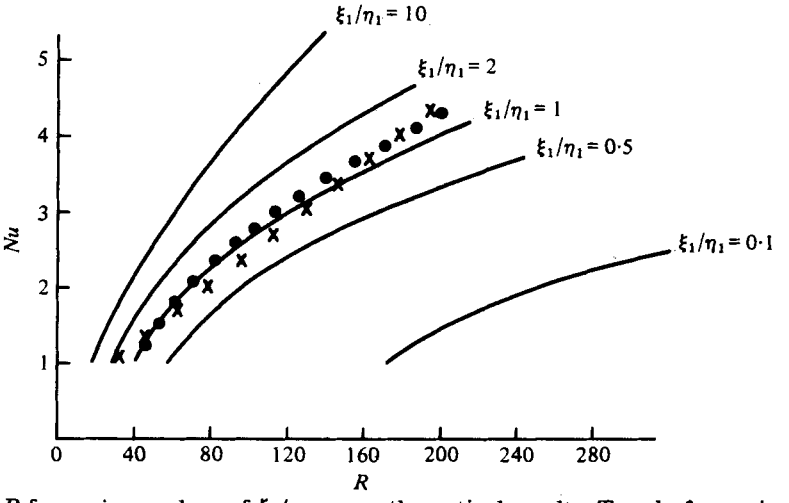

FIGURE 1. Nu *vs.* R for various values of ξ_1/η_1. ——, theoretical results. Trend of experimental results: ×, Castinel & Combarnous (1975) for $\xi_1/\eta_1 = 2{\cdot}08$; ●, Buretta (1972) for $\xi_1/\eta_1 = 1$.

To characterize the steady two-dimensional motion, we choose to concentrate on the Nusselt number. This is primarily because the heat transport is the most interesting physical quantity, but also because Nu is dependent on the anisotropy parameters only in the form ξ_1/η_1.

In figures 1–4 we have displayed some results for the Nusselt number. For every choice of R and ξ_1/η_1 we have chosen the wavenumber which gives the maximum value of Nu. The variation of the Nusselt number with the wavenumber in the regime of stable two-dimensional motion is within 5% for horizontally isotropic media (see Kvernvold 1975). For horizontally anisotropic media, however, the variation may be larger, because the rolls in this case are stable for a wider range of wavenumbers (see § 7).

Figure 1 shows Nu as a function of R for different values of ξ_1/η_1. We also display some results from experiments performed in anisotropic porous media by Castinel & Combarnous (1975) and some results from experiments in isotropic porous media by Buretta (1972). The results from the isotropy experiments fit well with our theoretical values. The results from the anisotropy experiments are, however, somewhat below the theoretical ones. We believe that this discrepancy is due to effects in the experimental set-up which does not satisfy the idealized theoretical model.

In figure 1 the main differences between the curves are due to the different critical Rayleigh numbers. This is a purely linear effect. To exhibit the nonlinear effects of

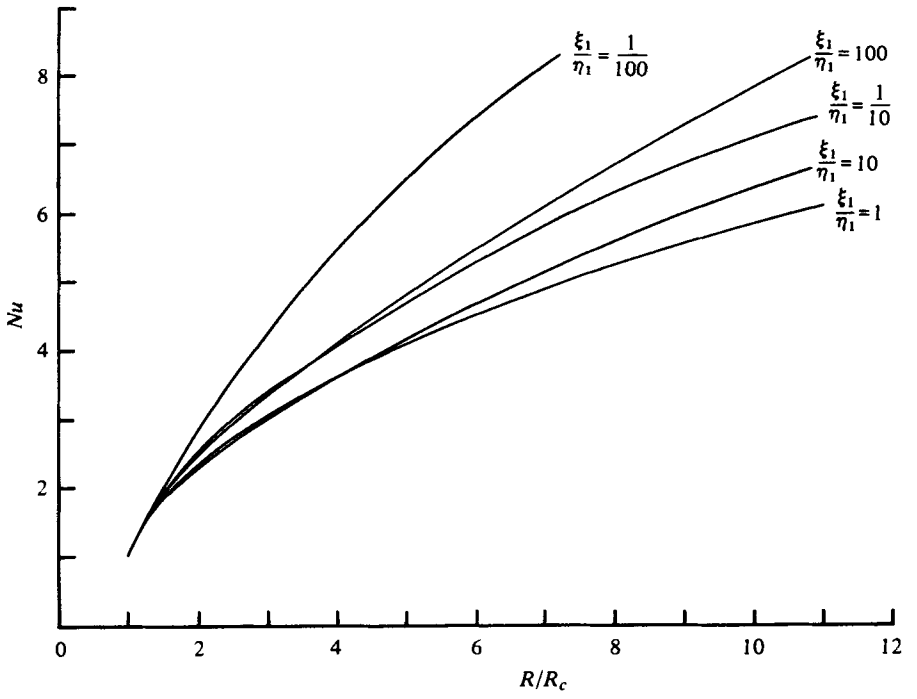

FIGURE 2. Nu *vs.* R/R_c for various values of ξ_1/η_1.

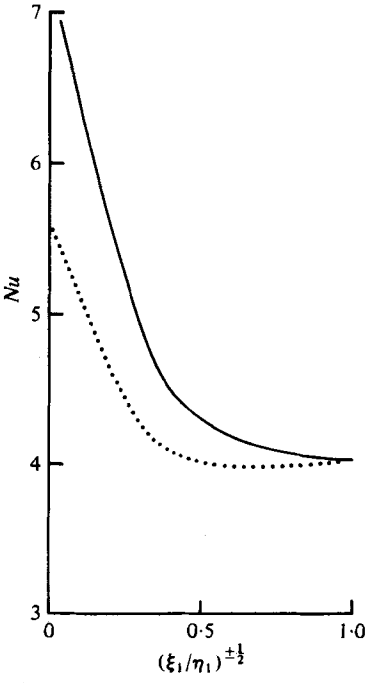

FIGURE 3. Nu as a function of ξ_1/η_1 for $R/R_c = 5{\cdot}0$. ——, Nu *vs.* $(\xi_1/\eta_1)^{\frac{1}{2}}$ for $0 < \xi_1/\eta_1 \leqslant 1$; ....., Nu *vs.* $(\xi_1/\eta_1)^{-\frac{1}{2}}$ for $1 \leqslant \xi_1/\eta_1 < \infty$.

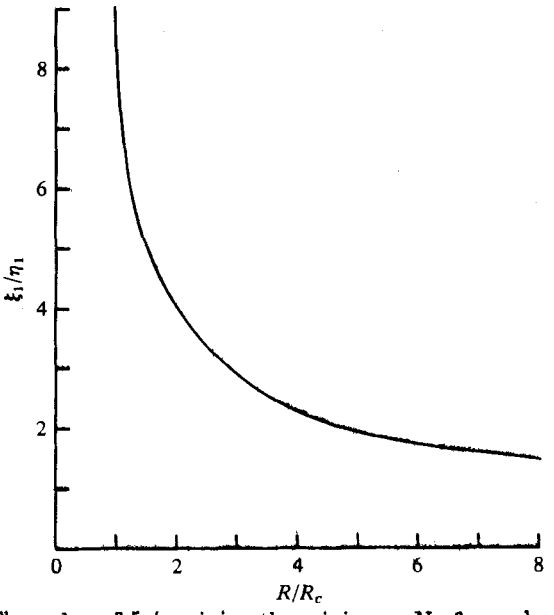

FIGURE 4. The value of ξ_1/η_1 giving the minimum Nu for each value of R/R_c.

anisotropy on the Nusselt number, in figure 2 we display Nu as a function of R/R_c. In the appendix we show analytically that all these curves start out with the same slope, independent of ξ_1/η_1. For moderate anisotropy and moderately supercritical Rayleigh number, the deviations from the isotropy curve are small.

In figure 3 we show the Nusselt number *vs.* ξ_1/η_1 for $R/R_c = 5{\cdot}0$. The qualitative features in figure 3 are the same for all relevant values of R/R_c: any value of ξ_1/η_1 larger than unity gives a larger Nusselt number than the corresponding inverse value. Furthermore, $\xi_1/\eta_1 \to 0$ yields the maximum Nusselt number. The value of ξ_1/η_1 which gives the minimum Nu does, however, vary with R/R_c. Figure 4 shows this variation. From the analytical results in the appendix it follows that minimum Nu when $R/R_c \to 1$ occurs for $\xi_1/\eta_1 = 9$.

6. Stability of the steady two-dimensional motion

It is of interest to determine the range of wavenumbers and Rayleigh numbers for which two-dimensional motion is stable with respect to small disturbances. We replace ψ by $\psi + \psi'$ in (4.5), where $\psi'(x, y, z, t)$ is a small disturbance of the steady solution. The equation for ψ' is linearized and becomes

$$\left[\left(\eta_1\frac{\partial^2}{\partial x^2}+\eta_2\frac{\partial^2}{\partial y^2}+\frac{\partial^2}{\partial z^2}-\frac{\partial}{\partial t}\right)\nabla^2+R\nabla_1^2\right]\psi' = \boldsymbol{\delta}\psi'\,.\,\nabla\nabla^2\psi+\boldsymbol{\delta}\psi\,.\,\nabla\nabla^2\psi', \tag{6.1}$$

with boundary conditions

$$\psi' = \psi'_{zz} = 0 \quad \text{at} \quad z = 0, 1. \tag{6.2}$$

If there exists a solution of (6.1) with growing time dependence, the steady solution is said to be unstable. Otherwise it is stable.

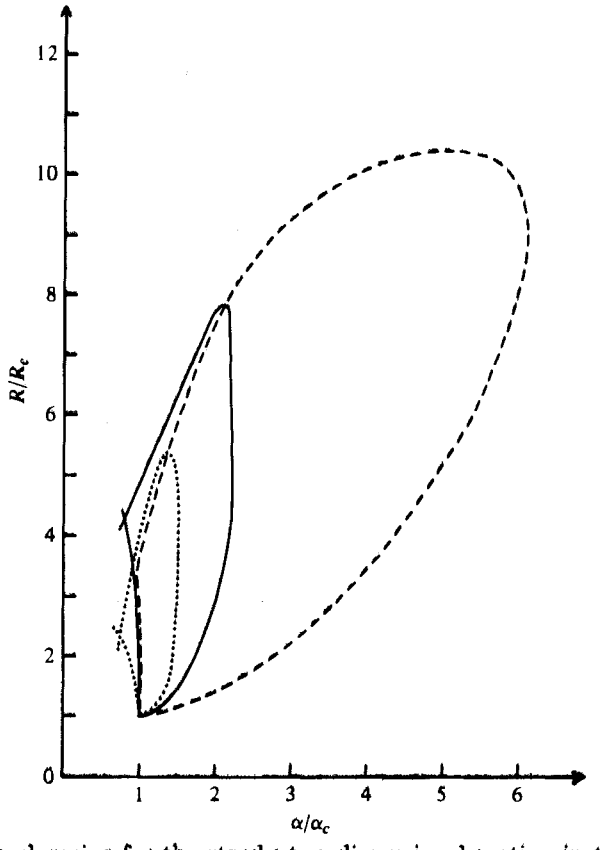

FIGURE 5. Stability domains for the steady two-dimensional motion in the α/α_c, R/R_c plane for selected values of ξ/η (horizontal isotropy). ——, $\xi/\eta = 1$; - - - -, $\xi/\eta = 100$; · · · ·, $\xi/\eta = \frac{1}{100}$.

The solution is written as

$$\psi' = \sum_{n,m} A'_{n,m} \exp(in\alpha x) \exp[i(dx+by)+\sigma t] \sin m\pi z. \tag{6.3}$$

The equations for the unknowns $A'_{n,m}$ are obtained by multiplying (6.1) by

$$\exp(-ip\alpha x) \exp[-i(dx+by)-\sigma t] \sin q\pi z$$

and averaging over the whole fluid layer. We neglect, as in the steady case, all terms with $|n|+\frac{1}{2}(m+1) > N$, where N has the same value as in the corresponding steady problem. The system of linear homogeneous equations constitutes an eigenvalue problem for σ. The analysis is simplified because the system separates into two sub-systems with $n+m$ even and $n+m$ odd, respectively.

The eigenvalue is given by

$$\sigma = \sigma(\alpha, R, b, d), \tag{6.4}$$

and for a given α and R, we have to vary both b and d to find the most unstable disturbances. Numerical results show that those occur for either $b = 0$ or $d = 0$. Disturbances with $b = 0$ have axes parallel to the axes of the steady rolls. The corresponding instability is referred to as Eckhaus instability. Disturbances with $d = 0$ give rise to instability which is termed cross-roll instability if b is of the same order of magnitude as α_c and zigzag instability if $b \to 0$.

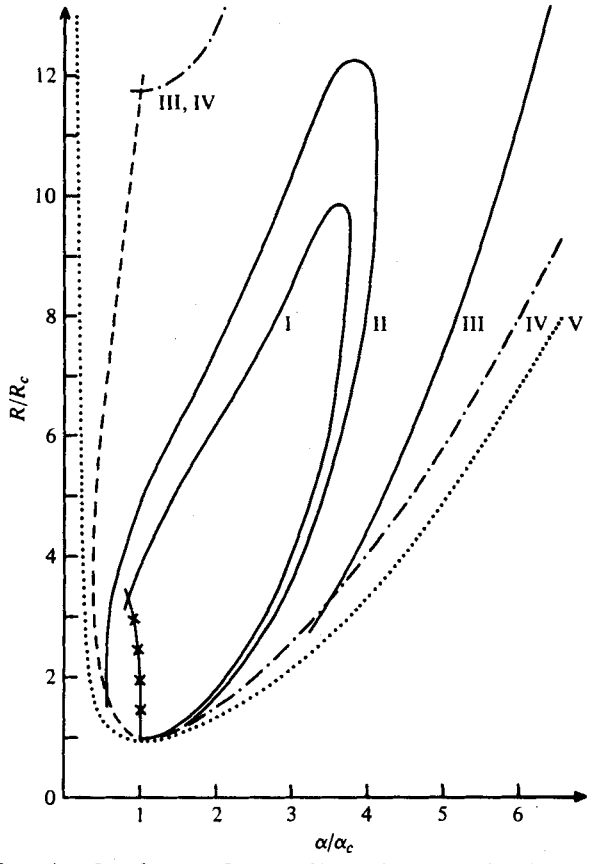

FIGURE 6. Stability domains for the steady two-dimensional motion in the α/α_c, R/R_c plane. I, horizontal isotropy, $\xi/\eta = 10$; II, $\xi_1/\eta_1 = 10$, $\xi_2/\eta_2 = 8$; III, $\xi_1/\eta_1 = 10$, $\xi_2/\eta_2 = 1$; IV, $\xi_1/\eta_1 = 10$, $\xi_2/\eta_2 = 0$; V, neutral curve for the onset of convection; ——, cross-roll instability; —×—, zig-zag instability; - - - - -, oscillatory Eckhaus instability; —·—, exponential Eckhaus instability.

We first consider the case of horizontal isotropy, defined by $\xi_1 = \xi_2 = \xi$, $\eta_1 = \eta_2 = \eta$. In this case it turns out that cross-rolls are the most unstable disturbances, except for a domain with $\alpha < \alpha_c$ and R moderately supercritical, where zigzag instability occurs. The stability regions for two rather extreme values of ξ/η ($\frac{1}{100}$ and 100) are shown in figure 5. For comparison the case of isotropy ($\xi/\eta = 1$) is also displayed. The domains of stability lie within closed curves, giving upper limits on the Rayleigh number for which steady two-dimensional motion is stable. No oscillatory instability will occur for horizontal isotropy. Values of ξ/η between the values represented on figure 5 give stability regions intermediate between the regions displayed. Except for a small discrepancy in the zigzag instability, the curve for isotropy is the same as those obtained by Straus (1974) and Kvernvold (1975).

Let us consider media which are horizontally anisotropic ($\xi_1/\eta_1 \geqslant \xi_2/\eta_2$). The steady motion is the same as for horizontally isotropic media with the same value of ξ_1/η_1. The stability is, however, fundamentally different. This is because the horizontal anisotropy makes cross-rolls and zigzags linearly stable in a certain domain of R/R_c, which is larger the more ξ_2/η_2 deviates from ξ_1/η_1. In this region the stability bounds are determined by Eckhaus instability, which is independent of ξ_2/η_2. Eckhaus

disturbances are generally more stable than cross-rolls. Consequently, a horizontally anisotropic medium has a larger stability region than a horizontally isotropic medium with the same steady solution.

A convenient way to demonstrate the effects of horizontal anisotropy on the stability domain is to keep ξ_1/η_1 fixed, which means that the steady problem is fixed, and allow ξ_2/η_2 to take values from zero to ξ_1/η_1. We shall display only one example, $\xi_1/\eta_1 = 10$ (figure 6), because the qualitative features are the same for other values of ξ_1/η_1. Here ξ_2/η_2 is given decreasing values. Starting with the horizontally isotropic case, $\xi_2/\eta_2 = 10$ (curve I), we get a stability domain consistent with those in figure 5. Curve II is given by $\xi_2/\eta_2 = 8$; the enlargement of the stability domain is already remarkable. Curve III is given by $\xi_2/\eta_2 = 1$; the left-hand branch of the stability domain is now determined by Eckhaus instability at least to $R/R_c = 14$. Curve IV represents the extreme case $\xi_2/\eta_2 = 0$; then only Eckhaus disturbances are possible. We observe that for horizontal anisotropy oscillatory Eckhaus instability may occur for $\alpha < \alpha_c$.

It is believed that, in all cases with ξ_2/η_2 non-zero, the cross-rolls will close the stability domain for finite values of R/R_c. The case $\xi_2/\eta_2 = 0$ may be interpreted as a generalized Hele–Shaw cell. The calculations show in this case no tendency to yield an upper limit beyond which two-dimensional motion is unstable. This is also supported by Horne & O'Sullivan (1974), who found steady motion in a Hele–Shaw cell for R up to $30R_c$ by a finite-element method.

7. Applications to insulation techniques

We shall use the above general results to discuss some aspects of the insulating properties of transversely isotropic porous materials, which we define to have equal permeabilities and thermal diffusivities in all directions normal to a specified direction. Let K_{I} and K_{II} denote the longitudinal and transverse permeability, respectively, and $\kappa_{m\mathrm{I}}$ and $\kappa_{m\mathrm{II}}$ the longitudinal and transverse effective diffusivity, respectively. Four typical examples of transversely isotropic media are sketched in figure 7.

Our aim is to minimize the loss of heat through a horizontal layer. In the conduction regime the heat transport is proportional to the vertical thermal diffusivity. It is therefore important to orientate the material such that minimum vertical diffusivity is achieved. Further, it is important to delay the onset of convection, because the occurrence of convection increases the total heat transport. For horizontal isotropy given by

$$\xi_1 = \xi_2 = K_{\mathrm{II}}/K_{\mathrm{I}}, \quad \eta_1 = \eta_2 = \kappa_{m\mathrm{II}}/\kappa_{m\mathrm{I}}, \tag{7.1}$$

the critical temperature difference is, from (3.12),

$$\Delta T_c = \frac{\nu\pi^2}{g\gamma h}\left[\left(\frac{\kappa_{m\mathrm{I}}}{K_{\mathrm{I}}}\right)^{\frac{1}{2}} + \left(\frac{\kappa_{m\mathrm{II}}}{K_{\mathrm{II}}}\right)^{\frac{1}{2}}\right]^2. \tag{7.2}$$

When the material is turned through 90° we get isotropy in, say, the x, z plane. Then

$$\xi_1 = K_{\mathrm{I}}/K_{\mathrm{II}}, \quad \eta_1 = \kappa_{m\mathrm{I}}/\kappa_{m\mathrm{II}}, \quad \xi_2 = \eta_2 = 1, \tag{7.3}$$

giving from (3.3)

$$\Delta T_c = \frac{\nu\pi^2}{g\gamma h}\left[\min\left\{\left(\frac{\kappa_{m\mathrm{I}}}{K_{\mathrm{I}}}\right)^{\frac{1}{2}}, \quad \left(\frac{\kappa_{m\mathrm{II}}}{K_{\mathrm{II}}}\right)^{\frac{1}{2}}\right\} + \left(\frac{\kappa_{m\mathrm{II}}}{K_{\mathrm{II}}}\right)^{\frac{1}{2}}\right]^2. \tag{7.4}$$

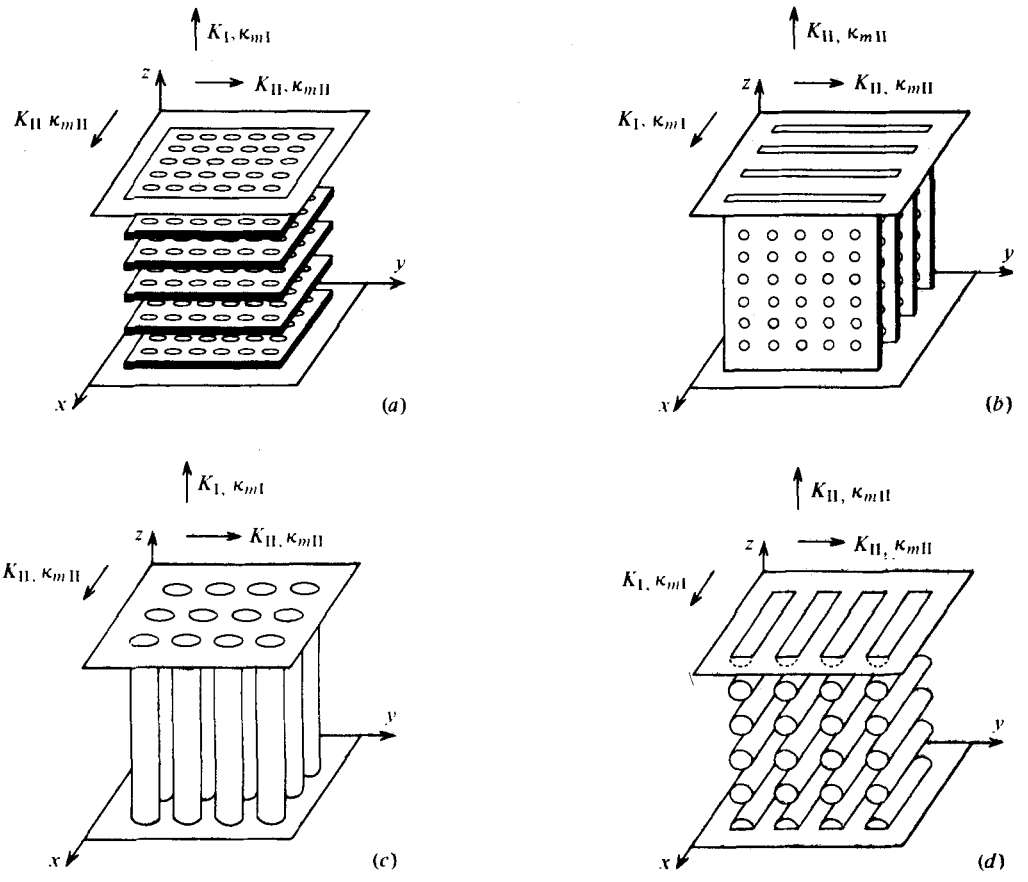

FIGURE 7. Sketches of transversely isotropic media composed of equally spaced, parallel perforated plates or parallel fibres. (*a*) Horizontal plates. (*b*) Vertical plates. (*c*) Vertical fibres. (*d*) Horizontal fibres.

The class of materials defined by

$$\kappa_{m\mathrm{I}}/K_{\mathrm{I}} > \kappa_{m\mathrm{II}}/K_{\mathrm{II}} \tag{7.5}$$

may appropriately be termed 'parallel perforated plates'; see figures 7(*a*) and (*b*). Equations (7.2) and (7.4) imply that horizontal plates have a larger critical temperature difference than vertical plates.

The other class of materials, defined by

$$\kappa_{m\mathrm{I}}/K_{\mathrm{I}} \leqslant \kappa_{m\mathrm{II}}/K_{\mathrm{II}}, \tag{7.6}$$

will be termed 'parallel fibres'; see figures 7(*c*) and (*d*). The critical temperature difference is the same for horizontal and vertical fibres.

The dimensionless heat transport after the onset of convection is measured by the Nusselt number. Figure 2 shows that the Nusselt number dependence on R/R_c is different for different anisotropy. It is, however, the dimensional heat transport which is of importance from a physical point of view. But, because of the different effects involved in the heat transport, further conclusions can be given only for special cases.

An interesting special case is a thermally isotropic material ($\kappa_{m\mathrm{I}} = \kappa_{m\mathrm{II}}$). This is a

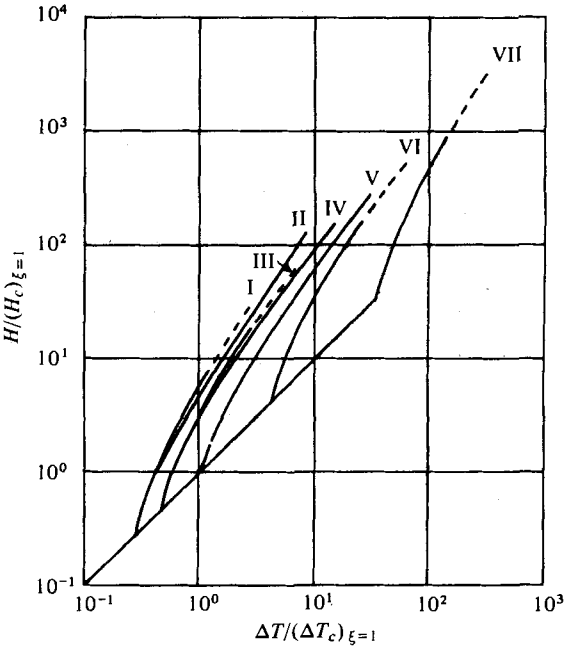

FIGURE 8. Comparison of the heat flux *vs.* temperature difference for transversely isotropic media with equal, isotropic diffusivities and K_{II} kept fixed. I, $K_I/K_{II} = 100$, longitudinal direction vertical; II, $K_I/K_{II} = 100$, horizontal; III, $K_I/K_{II} = 10$, vertical; IV, $K_I/K_{II} = 10$, horizontal; V, $K_I/K_{II} \leqslant 1$, horizontal; VI, $K_I/K_{II} = \frac{1}{10}$, vertical; VII, $K_I/K_{II} = \frac{1}{100}$, vertical; – – –, two-dimensional steady motion unstable.

good approximation for most insulation materials. In this case we conclude the following.

(i) Horizontal fibres always allow less heat transport than the same fibres turned vertically. The critical temperature difference is the same, and the difference in heat transport is solely due to the difference in Nusselt number as given by figure 3.

(ii) For perforated plates the problem is more complicated. The Nusselt number for horizontal plates is given by the lower branch (dotted curve) in figure 3. It is less than the Nusselt number for vertical plates when K_I/K_{II} is small and greater when K_I/K_{II} is large. The Nusselt number for vertical plates is the same as for isotropy. The critical temperature difference is, however, larger for horizontal plates than for vertical plates, so that the total heat transport (conduction + convection) is always greater for vertical plates than for horizontal plates. This is evident from figure 8, where we have displayed the heat flux *vs.* the temperature difference for various values of K_I with K_{II} and $\kappa_{mI} = \kappa_{mII}$ constant. Curve V gives the heat flux for vertical plates, while curves VI and VII give the heat flux for two types of horizontal plates. From this figure we conclude that the type of thermally isotropic medium which gives the best insulation is a horizontally isotropic medium with as small a vertical permeability as possible.

The above conclusions are strictly valid only in the regions where two-dimensional motion is stable. However, both experiments (Krishnamurti 1970) and theory (Tveitereid 1977) indicate that the heat transport is nearly independent of the horizontal planform. We therefore expect the heat transport given by the two-dimensional

solution to have a quantitatively acceptable value even for Rayleigh numbers in the unstable regime.

8. Summary

A theoretical analysis of thermal convection in anisotropic porous media has been performed. The criterion for the onset of convection was derived. Moreover, the supercritical steady two-dimensional motion was investigated both numerically and analytically, and regions of stable wavenumbers and Rayleigh numbers were found.

It was shown that the Nusselt number and the stability regions depend on the anisotropy parameters only through the ratios ξ_1/η_1 and ξ_2/η_2. The velocity and temperature fields, however, depend on the appropriate values of ξ_1, ξ_2, η_1 and η_2.

From figure 2 we observe that the nonlinear effects of anisotropy on the Nusselt number are not very pronounced. Actually, all curves of Nu *vs.* R/R_c start out with the same slope. The linear effects of anisotropy are usually much more important, as shown in figures 1 and 8. Figure 8 illustrates the problem of orientating a given porous material in order to minimize the heat transport. It has a bearing on insulation techniques, and this aspect is discussed separately.

The steady two-dimensional motion is the same for both horizontally anisotropic and horizontally isotropic media (for the same ξ_1/η_1). The stability regions are, however, of different character. For horizontal isotropic media (case C) the stability regions do not differ qualitatively from the results obtained for fully isotropic porous material by Straus (1974) and Kvernvold (1975). For horizontally anisotropic media (cases A and B) the orientation of a roll is determined by the linear theory. The steady two-dimensional motion is now stable for a wider range of wavenumbers and Rayleigh numbers than in the corresponding problem of horizontally isotropic media; see figure 6. This is because horizontal anisotropy renders cross-rolls linearly stable in a certain supercritical domain of R/R_c. This domain is larger the more ξ_1/η_1 differs from ξ_2/η_2.

The authors wish to thank Dr M. Tveitereid and Dr J. E. Weber for valuable discussions during the preparation of this paper.

Appendix

Near the critical Rayleigh number, the problem may be solved analytically by the method introduced by Kuo (1961) and applied by Palm *et al.* (1972). The expansion parameter ϵ is defined by

$$\epsilon^2 = (R - R_c)/R, \tag{A 1}$$

giving

$$R = R_c/(1-\epsilon^2) = R_c + R_{cs}(\epsilon^2 + \epsilon^4 + \ldots + \epsilon^{2s}), \tag{A 2}$$

where

$$R_{cs} = R_c/(1-\epsilon^{2s}). \tag{A 3}$$

The calculation follows closely that of Palm *et al.* (1972), but is performed to only fourth order. The advantage of expressing R as the finite sum (A 2) is to improve the convergence of the method; see Palm *et al.* (1972). Following Kuo's idea we choose $s = N$ when solving the system to order $2N$. With this choice of s, (A 2) gives an exact representation of R.

R/R_c \ ξ_1/η_1		0	0·01	0·1	1	9	∞
1·2	Analytical	1·421	1·387	1·369	1·360	1·357	1·364
	Numerical	—	1·382	1·363	1·352	1·350	—
1·5	Analytical	2·094	1·943	1·865	1·823	1·813	1·844
	Numerical	—	1·910	1·808	1·757	1·747	—
2·0	Analytical	3·250	2·849	2·641	2·528	2·500	2·583
	Numerical	—	2·658	2·383	2·251	2·234	—

TABLE 2. Analytical and numerical results for the Nusselt number ($\alpha = \alpha_c$).

The solution of (4.6) subject to the boundary conditions (4.7) is written as

$$\psi = \sum_{n=1}^{\infty} \epsilon^n \psi^{(n)}, \tag{A 4}$$

where

$$\psi^{(n)} = A_n \cos \alpha x \sin \pi x + \sum_{p,q} B_{pq}^{(n)} \cos p\alpha x \sin q\pi z. \tag{A 5}$$

Here α is the horizontal wavenumber, which will be chosen equal to the critical wavenumber in this analytical calculation. The amplitudes A_n are determined from the solvability conditions on the inhomogeneous differential equation to each order in ϵ, which give

$$A_1 = \left[\frac{8}{\pi^2}\frac{R_{cs}}{R_c}\eta_1(\eta_1^{\frac{1}{2}}+1)\right]^{\frac{1}{2}}, \tag{A 6a}$$

$$A_3 = \left[\frac{8}{\pi^2}\frac{R_{cs}}{R_c}\eta_1(\eta_1^{\frac{1}{2}}+1)\right]^{\frac{1}{2}}\left(\tfrac{1}{2}+\frac{1}{16}\frac{R_{cs}}{R_c}\frac{11\eta_1+14\eta_1^{\frac{1}{2}}+3}{\eta_1+10\eta_1^{\frac{1}{2}}+1)}\right), \tag{A 6b}$$

$$A_2 = A_4 = 0. \tag{A 6c}$$

Further,

$$B_{nq}^{(n)} = B_{nq}^{(n)}(A_1, \ldots, A_{n-1}). \tag{A 7}$$

Let $Nu^{(2)}$ and $Nu^{(4)}$ denote the Nusselt number to second and fourth order, respectively. The anisotropy in permeability is now incorporated in the results, i.e. η_1 is replaced by η_1/ξ_1:

$$Nu^{(2)} = 1 + 2\frac{R_{cs}}{R_c}\epsilon^2, \tag{A 8}$$

$$Nu^{(4)} = Nu^{(2)} + 2\frac{R_{cs}}{R_c}\left(1+\frac{1}{8}\frac{3\eta_1/\xi_1 - 66(\eta_1/\xi_1)^{\frac{1}{2}} - 5}{\eta_1/\xi_1 + 10(\eta_1/\xi_1)^{\frac{1}{2}}+1}\frac{R_{cs}}{R_c}\right)\epsilon^4. \tag{A 9}$$

The expression for $Nu^{(2)}$ shows that all curves for Nu *vs.* R/R_c start out with the same slope, independent of ξ_1/η_1. In table 2 we give some results for $Nu^{(4)}$ for $s = 2$ and different values of R/R_c and ξ_1/η_1. For comparison the corresponding results of the numerical calculation are also quoted. The table shows satisfactory agreement between numerical and analytical results for $R/R_c < 1{\cdot}5$. The minimum and maximum values of $Nu^{(4)}$ occur for $\xi_1/\eta_1 = 9$ and $\xi_1/\eta_1 \to 0$, respectively.

REFERENCES

BEAR, J. 1972 *Dynamics of Fluids in Porous Media*. Elsevier.

BURETTA, R. 1972 Ph.D. dissertation, University of Minnesota.

BURNS, P. J., CHOW, L. C. & TIEN, C. L. 1977 *Int. J. Heat Mass Transfer* **20**, 919.

BUSSE, F. H. 1967 *J. Math. Phys.* **46**, 140.

CASTINEL, G. & COMBARNOUS, M. 1975 *Rev. Thermique* **168**, 937.

ELDER, J. W. 1967 *J. Fluid Mech.* **27**, 29.

EPHERRE, J. F. 1975 *Rev. Thermique* **168**, 949.

HORNE, R. N. & O'SULLIVAN, M. J. 1974 *J. Fluid Mech.* **66**, 339.

KRISHNAMURTI, R. 1970 *J. Fluid Mech.* **42**, 295.

KUO, H. L. 1961 *J. Fluid Mech.* **10**, 611.

KVERNVOLD, O. 1975 *Univ. Oslo Preprint Ser.* no. 1.

NEALE, G. 1977 *A.I.Ch.E. J.* **23**, 56.

PALM, E., WEBER, J. E. & KVERNVOLD, O. 1972 *J. Fluid Mech.* **45**, 153.

SCHLÜTER, A., LORTZ, D. & BUSSE, F. 1965 *J. Fluid Mech.* **23**, 129.

STRAUS, J. M. 1974 *J. Fluid Mech.* **64**, 51.

TVEITEREID, M. 1977 *Int. J. Heat Mass Transfer* **20**, 1045.

TYVAND, P. A. 1977 *J. Hydrol.* **34**, 335.